frontiers | Frontiers in Astronomy and Space Sciences

TYPE Original Research
PUBLISHED 15 August 2022
DOI 10.3389/fspas.2022.975123

OPEN ACCESS

EDITED BY
Xiao-Jia Zhang,
University of California, Los Angeles, United States

REVIEWED BY
Anton Artemyev,
Department of Earth, Planetary, and Space Sciences, College of Physical Sciences, University of California, Los Angeles, United States
Toshi Nishimura,
Boston University, United States

*CORRESPONDENCE
Mykhaylo Shumko,
msshumko@gmail.com

SPECIALTY SECTION
This article was submitted to Space Physics, a section of the journal Frontiers in Astronomy and Space Sciences

RECEIVED 21 June 2022
ACCEPTED 18 July 2022
PUBLISHED 15 August 2022

CITATION
Shumko M, Gallardo-Lacourt B, Halford AJ, Blum LW, Liang J, Miyoshi Y, Hosokawa K, Donovan E, Mann IR, Murphy K, Spanswick EL, Blake JB, Looper MD and Gillies DM (2022), Proton aurora and relativistic electron microbursts scattered by electromagnetic ion cyclotron waves. *Front. Astron. Space Sci.* 9:975123. doi: 10.3389/fspas.2022.975123

Proton aurora and relativistic electron microbursts scattered by electromagnetic ion cyclotron waves

Mykhaylo Shumko[1,2]*, Bea Gallardo-Lacourt[1,3], Alexa Jean Halford[1], Lauren W. Blum[4], Jun Liang[5], Yoshizumi Miyoshi[6], Keisuke Hosokawa[7], Eric Donovan[5], Ian R. Mann[8], Kyle Murphy, Emma L. Spanswick[5], J. Bernard Blake[9], Mark D. Looper[9] and D. Megan Gillies[5]

[1]NASA's Goddard Space Flight Center, Greenbelt, MD, United States, [2]Department of Astronomy, University of Maryland, College Park, MD, United States, [3]Department of Physics, The Catholic University of America, Washington, DC, United States, [4]University of Colorado in Boulder, Boulder, Colorado, United States, [5]University of Calgary in Calgary, Calgary, AB, Canada, [6]Institute for Space-Earth Environmental Research, Nagoya University, Nagoya, Japan, [7]University of Electro-Communications, Tokyo, Japan, [8]University of Alberta in Edmonton, Edmonton, AB, Canada, [9]The Aerospace Corporation, Los Angeles, CA, United States

Charged particle precipitation from Earth's magnetosphere results in stunning displays of the aurora and energy transfer into the atmosphere. Some of this precipitation is caused by wave-particle interactions. In this study, we present an example of a wave-particle interaction between Electromagnetic Ion Cyclotron waves, and magnetospheric protons and electrons. This interaction resulted in a co-located isolated proton aurora and relativistic electron microbursts. While isolated proton aurora is widely believed to be caused by Electromagnetic Ion Cyclotron waves, this unique observation suggests that these waves can also scatter relativistic electron microbursts. Theoretically, nonlinear interactions between Electromagnetic Ion Cyclotron waves and electrons are necessary to produce the intense sub-second microburst precipitation. Lastly, detailed analysis of the auroral emissions suggests that no chorus waves were present during the event. This is in contrast to the most commonly associated driver of microbursts, whistler mode chorus waves, and supports other less commonly considered driving mechanisms.

KEYWORDS

EMIC, SAMPEX, THEMIS, microburst, proton aurora, all-sky-imager

1 Introduction

Since the Van Allen radiation belts were discovered by Van Allen (1959) and Vernov and Chudakov (1960), the loss of radiation belt electrons due to wave-particle interactions has been modeled with quasilinear diffusion theory (e.g., Kennel and Petschek, 1966; Summers et al., 1998; Summers, 2005; Thorne et al., 2005). On long time scales, this model leads to accurate quantification of particle energization and loss (e.g., Lyons and Thorne, 1973; Claudepierre et al., 2020). On shorter time scales, however, quasilinear diffusion does not accurately predict precipitating fluxes on second or sub-second timescales (e.g., Bortnik et al., 2008; Albert and Bortnik, 2009; Saito et al., 2012; Miyoshi et al., 2015; Mozer et al., 2018; Shumko et al., 2018). The importance of nonlinear scattering in regard to particle loss is still unknown. Indeed, even the variety of mechanisms that nonlinearily scatter radiation belt electrons is still unknown (e.g. Grach and Demekhov, 2020; Bortnik et al., 2022). Scattering mechanisms that lead to electron microburst precipitation are of particular interest here; while there is a plethora of observational evidence linking whistler mode chorus waves to electron microbursts, only Douma et al. (2018) shows observational evidence of microbursts scattered by Electromagnetic Ion Cyclotron (EMIC) waves.

Microbursts are intense bursts of electron precipitation that typically last ≈ 100 ms (Shumko et al., 2021). Microburst energies span from tens of keV all the way up to > 1 MeV (Anderson and Milton, 1964; Parks, 1967; O'Brien et al., 2003; Blum et al., 2015; Douma et al., 2017; Shumko et al., 2020b; Kawamura et al., 2021; Shumko et al., 2021; Zhang et al., 2022). The microburst L-MLT distribution peaks in the outer radiation belt L-shells and in the 0–12 MLT region (Lorentzen et al., 2001; O'Brien et al., 2003).

Whistler mode chorus waves share many similarities with microbursts, including similar distribution in MLT and duration (of chorus rising tone elements) (Teng et al., 2017; Meredith et al., 2020; Shumko et al., 2021). These similarities led to a widely-accepted conclusion that microbursts are most often scattered by whistler mode chorus waves (e.g., Lorentzen et al., 2001). This is further supported by theory. Both Miyoshi et al. (2020) and Chen et al. (2020) show that rising tone whistler mode chorus waves can rapidly—and nonlinearly—scatter microburst electrons over the wide range of energies.

EMIC waves are an another type of plasma wave that can pitch angle scatter energetic protons and electrons into Earth's atmosphere (e.g., Cornwall, 1965; Summers et al., 1998; Spasojević et al., 2004; Jordanova, 2007; Halford et al., 2016; Yahnin et al., 2021). EMIC waves are typically generated near the magnetic equator by anisotropic ions and are often bounded in frequency by the ion gyrofrequencies into three primary bands: hydrogen, helium, and oxygen (e.g., Gary et al., 1995; Blum et al., 2012; Saikin et al., 2015). In the magnetosphere, EMIC waves are spatially confined in L-Shell and extended in MLT (Mann et al., 2014; Blum et al., 2017). When some of the EMIC wave power enters the ionosphere, it can duct and be observed over a large geographical area (Woodroffe and Lysak, 2012; Mann et al., 2014; Kim et al., 2018).

During their generation and subsequent propagation away from the magnetic equator, EMIC waves can precipitate 10 s keV protons (e.g., Miyoshi et al., 2008; Shoji and Omura, 2011). When the protons impact the atmosphere, they decelerate via charge-exchange: the bare proton strips an electron from an atmospheric molecule and becomes a neutral hydrogen atom in an excited state (Kivelson et al., 1995). This hydrogen atom, newly decoupled from the magnetic field, then emits hydrogen-specific auroral light, primarily in the Lyman-α (121.57 nm), Balmer-α (653.3 nm), and Balmer-β (486.1 nm) lines (e.g., Gallardo-Lacourt et al., 2021). Davidson (1965) and Fang et al. (2004) show that this charge exchange process will spatially smear a fine beam of precipitating protons into a ≈ 100 km radius proton aurora patch.

Similarly, EMIC waves can also scatter relativistic electrons (e.g., Summers et al., 1998; Khazanov et al., 2014; Kubota et al., 2015; Remya et al., 2015; Zhang X.-J. et al., 2016; Kubota and Omura, 2017; Zhu et al., 2020; Grach et al., 2021). The theoretical work by Omura and Zhao (2013) is most relevant here: they demonstrated that EMIC waves can scatter relativistic microbursts into the atmosphere. There, these precipitating electrons experience bremsstrahlung deceleration and emit X-ray photons which are absorbed before they reach the ground (Winckler et al., 1958; Woodger et al., 2015). Therefore, relativistic electron precipitation can only be observed directly in space and indirectly via the secondary X-rays in the upper atmosphere.

Some satellites in low Earth orbit (LEO) are well-equipped to observe this dual electron-proton precipitation that is often attributed to EMIC wave scattering (e.g., Miyoshi et al., 2008; Nishimura et al., 2014; Zhang J. et al., 2016; Qin et al., 2018; Capannolo et al., 2021). These studies often show EMIC precipitation structure that lasts a few to 10s of seconds. From the vantage point of a high-inclination satellite in LEO, these durations can correspond to either the spatial size or temporal duration (Shumko et al., 2020a,b). Nevertheless, EMIC-driven electron precipitation on faster time scales is seldom observed. In fact, Douma et al. (2018) is the only study to our knowledge which shows sub-second electron precipitation associated with an EMIC wave. These authors presented the results of a magnetic conjunction between the Solar Anomalous and Magnetospheric Particle Explorer (SAMPEX) satellite in the northern hemisphere and a ground-based magnetometer in Halley, Antarctica. During the conjunction, SAMPEX observed three > 1 MeV electron microbursts.

Due to the aforementioned EMIC wave ducting and a lack of auroral observations, it is difficult to co-locate the EMIC wave and microbursts in the Douma et al. (2018) conjunction. However, observing an EMIC wave on the ground, together

with co-located proton and electron precipitation, will provide more convincing evidence of EMIC-driven electron microbursts. We present such a study here.

Early on 20 January 2007, the Canadian Array for Real-time Investigations of Magnetic Activity (CARISMA) magnetometers spread throughout Canada observed an EMIC wave lasting almost 2 hours. This wave generated an isolated proton aurora (IPA) patch that was observed by a Time History of Events and Macroscale Interactions during Substorms (THEMIS) all-sky imager (ASI) and a meridional scanning photometer. Meanwhile, the SAMPEX satellite passed directly through the proton aurora and observed very rapid and intense >1 MeV electron microbursts.

2 Materials and methods

2.1 Instruments

2.1.1 Canadian array for real-time investigations of magnetic activity

We used the CARISMA (Mann et al., 2008) magnetometers to identify EMIC waves. The instruments consist of fluxgate and induction coil magnetometers deployed throughout Canada. Here we use the fluxgate magnetometer from Gillam (CARISMA-GILL) that is close to the ASI that observed the proton aurora. The magnetometer data is collected in two modes: 1- and 8-Hz sample rates. We use the 1-Hz data here.

2.1.2 Solar anomalous and magnetospheric particle explorer

We used the SAMPEX satellite to identify relativistic microbursts. It was launched in July 1992 into a 520, −, 760 km altitude, 82° inclination low Earth orbit (Baker et al., 1993; 2012). The Heavy Ion Large Telescope (HILT; Klecker et al., 1993) observed >1 MeV electrons. HILT was a large rectangular chamber with the aperture on one end, and 16 solid state detectors on the other. During this event HILT pointed to zenith and the electron counts were accumulated from all of the solid state detectors at a 20 ms cadence.

2.1.3 Time history of events and macroscale interactions during substorms all-sky imager

We use the THEMIS ASIs to study the auroral light. The THEMIS ASIs are an array of charged-coupled device (CCD) auroral cameras spread across Canada and Alaska (Harris et al., 2009; Mende et al., 2009). Each white light imager uses a fisheye lens to expand its field of view to 170°, corresponding to 9° latitudinal and 1 h magnetic local time (MLT) coverage (Donovan et al., 2006; Mende et al., 2009).

The 256 × 256 pixel images are taken at a 3-s cadence: a 1-s exposure is followed by 2-s processing. To analyze the white light images, we used the THEMIS ASI skymap calibration files that are provided by the University of Calgary. The calibration data contain, among other things, arrays that map each pixel to (latitude, longitude) coordinates at an assumed auroral emission altitude.

In this study, we use the THEMIS ASI camera stationed in The Pas (THEMIS-TPAS) to study the proton aurora. Furthermore, we briefly use the THEMIS ASI at Gillam (THEMIS-GILL) to identify the proton aurora, but the aurora was overwhelmed by light pollution in that part of THEMIS-GILL's sky.

2.1.4 Meridian scanning photometer

And lastly, we used the Northern Solar Terrestrial Array (NORSTAR) meridian scanning photometers (MSPs) to understand the multispectral properties of the aurora. MSPs are designed to measure the latitudinal location and brightness of aurora at the meridian. We use four channels from the MSP at Gillam (MSP-GILL): 470.9 nm blue-line, 486.0 nm H_β (i.e.. the Balmer-β emission line), 557.7 nm green-line, and 630 nm red-line (Jackel, 2005). See Unick et al. (2017) for a comprehensive description of the operation and calibration of MSPs.

2.2 Methods

Our analysis consists of two main steps: calculate the CARISMA wave spectrum, and map the THEMIS-TPAS images and SAMPEX footprints to 110 km altitude.

To calculate the CARISMA frequency-time spectrum, we used the Windowed Fast Fourier Transform algorithm implemented by Scipy's spectrogram ()function (Virtanen et al., 2020). We used the Tukey window (also known as the tapered cosine) that had a 256-s length. The windows overlapped by 128 s (50% of the window length).

Then, to accurately compare the two datasets, we mapped the THEMIS-TPAS ASI images and the SAMPEX location to the same altitude. For the images, we mapped the THEMIS-TPAS pixels along their line of sight to their (latitude, longitude) at a 110 km altitude. We used the aforementioned skymap files, together with Python's pymap3d (Hirsch, 2016), and aurora-asi-lib (Shumko, 2022) libraries to do this. For SAMPEX, we mapped its location to its magnetic field footprint at 110 km altitude. For this we used the IRBEM-Lib magnetic field library (Boscher et al., 2012) with the IGRF magnetic field model (Thébault et al., 2015).

3 Results

From approximately 00:00–01:40 UT on 20 January 2007, nine CARISMA magnetometers deployed around central Canada observed EMIC wave power between 0.25–0.4 Hz, classified as Pc

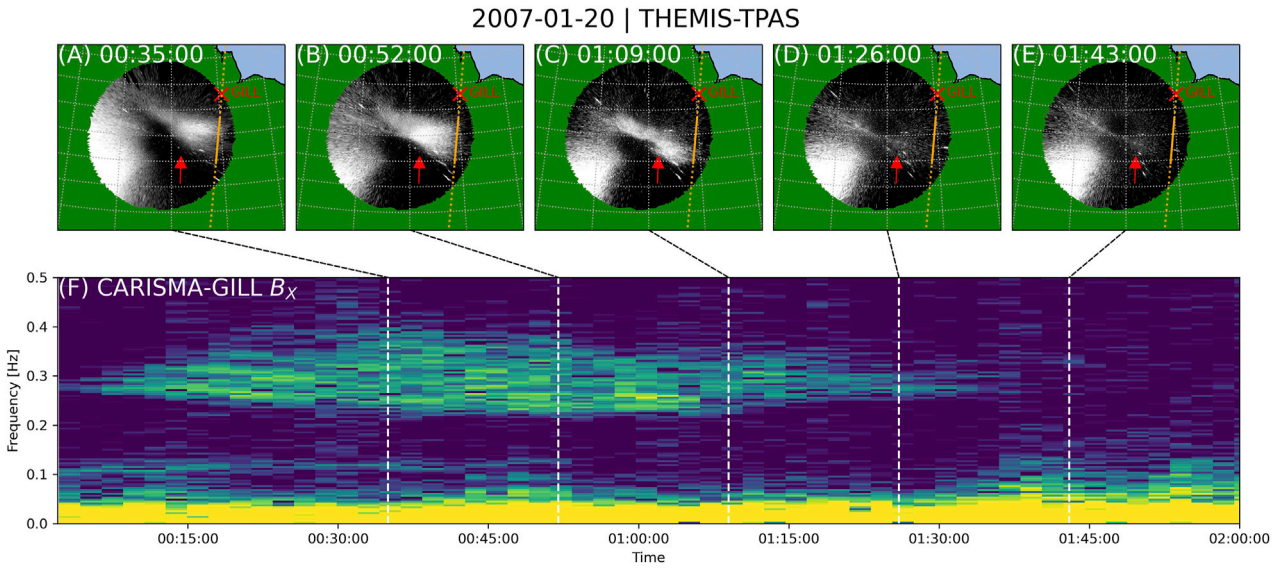

FIGURE 1
Select ASI images and magnetic field spectrum from the first 2 hours on 2007–01-20. **(A–E)** show select THEMIS ASI images from The Pas (TPAS). The intensity bounds are identical between the panels. Light pollution from twilight and other terrestrial sources is in the lower-left corner (south-west). The red arrows point to the proton aurora that the imager observed in **(A–C)**. The red X shows the location of the ASI and MSP at Gillam. The dotted orange line shows the GILL-MSP field of view, with the solid orange highlighting the 62° – 65° magnetic latitudes. **(F)** shows the B_X component of the magnetic field variations observed by a CARISMA magnetometer in Gillam. The proton aurora coincided with the EMIC wave in **(A–C)**, after which the magnetic wave power and proton aurora simultaneously faded in **(D,E)**.

1 (Jacobs et al., 1964). Figure 1F and Supplementary Video S1 show the EMIC wave observed at CARISMA-GILL. The primary band of the EMIC wave spanned 0.25–0.4 Hz. A second weaker band, centered around 0.1 Hz, ended earlier around 01:00 UT. Supplementary Figure S1 shows the spatial extent of the EMIC wave as observed on the ground: it shows a map of Canada with the CARISMA magnetometer locations that observed EMIC waves highlighted. The EMIC wave amplitude was largest at the Island Lake magnetometer (CARSIMA-ISLL), 275 km south of CARISMA-GILL. The wave appeared to be almost linearly polarized with the semi-major axis pointing north, suggesting that the EMIC wave entered the ionosphere near ISLL (Woodroffe and Lysak, 2012).

The 0.25–0.4 Hz EMIC wave band coincided with an auroral patch that was observed concurrently by two THEMIS ASIs located at Gillam (GILL) and The Pas (TPAS). The ASIs observed the aurora from just after the cameras turned on at sunset until 01:40 UT. THEMIS-TPAS is 500 km south-west of THEMIS-GILL and the auroral patch was observed in between the two imagers. While THEMIS-TPAS observed the patch in the region of the sky away from sunset, THEMIS-GILL observed the aurora light superposed with a strong background light consisting of twilight and terrestrial light. Thus, our analysis focused on THEMIS-TPAS. At TPAS the sunset was at 23:03 UT the previous day and twilight lasted until 01:09 UT on January 20th. The TPAS imager turned on at 00:22:06 UT and was initially saturated by twilight. The image in Figure 1A, taken at 00:35 UT, was the earliest time when the auroral patch was clearly visible. Panels (E) and (F) in Figure 1 show that both the auroral patch and EMIC waves vanished simultaneously around 01:45 UT, indicating that the auroral patch was driven by the EMIC wave.

Next, we investigate what particles created the auroral patch light. Figure 2 shows a multi-spectral keogram from MSP-GILL in panels (A)-(D) and a THEMIS-TPAS keogram along MSP-GILL's field of view in panel (E). We show MSP-GILL's field of view at 110 km altitude in Figures 1A–E with the dotted orange line. Figures 2A–D shows that the green and H_β MSP channels observed an intensity enhancement corresponding to magnetic latitudes $\lambda = 62°–65°$ that we highlighted in Figures 1A–E with the solid orange line. The H_β MSP channel is sensitive to precipitating 10 s keV protons, while the green MSP channel is sensitive to secondary electrons that were generated by the protons (Sakaguchi et al., 2008). While the aurora intensity was dim in the H_β channel, we confirmed that it was not observed in the MSP's 480 and 495 nm background channels.

Since we're using THEMIS-TPAS images, we need to compare its light to MSP-GILL to identify the proton emission. Figure 2E shows a keogram constructed along the MSP-GILL field of view using data extracted from the THEMIS-TPAS ASI images. The field of view grazed the auroral patch that THEMIS-TPAS observed—enough that the two can be

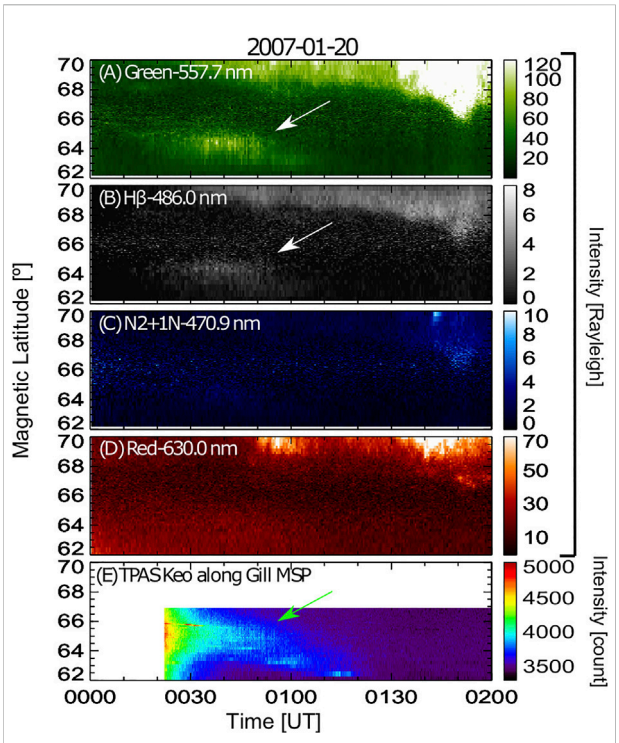

FIGURE 2
Keograms from Gillam and The Pas. **(A–D)** show the MSP intensity in the H_β, blue, and red channels. **(E)** shows a keogram constructed along the MSP-GILL field of view using data extracted from the THEMIS-TPAS ASI images. The matching aurora intensity in **(A,B,E)** confirm that the aurora observed by THEMIS-TPAS right after sunset was generated by protons.

compared. The auroral patch observed by THEMIS-TPAS was constrained to $\lambda = 62^\circ$–65° along the MSP's field of view. Thus, the auroral patch seen in the ASI images was caused by the precipitating 10 s keV protons, confirmed with the MSP-GILL, and is an IPA.

At 00:40 UT SAMPEX orbited above the IPA and directly observed precipitating relativistic electrons. Supplementary Video S1 and Figure 3 show the conjunction that was at approximately L = 5 and MLT = 17 h. Figures 3A–D shows the mapped THEMIS-TPAS image with the SAMPEX orbit footprint superposed as a dotted red line and the instantaneous footprint as a red circle. Figure 3E shows that HILT observed a handful of >1 MeV electron microbursts. We used the fitting method described in Shumko et al. (2021) to estimate microburst durations. Some of the microbursts lasted ≈ 100 ms, while three had a ≈ 300 ms duration.

Two more instruments onboard SAMPEX, the Proton/Electron Telescope (PET; Cook et al., 1993) and the Low-Energy Ion Composition Analyzer (LICA; Mason et al., 1993), observed precipitation at this time that we show in Supplementary Figure S2. PET is sensitive to >400 keV electrons and clearly observed many microbursts at a 100 ms cadence. Electron precipitation was also observed by LICA's stop microchannel plate that was sensitive to >25 keV electrons. However, LICA's time resolution was 1 s, so microbursts are difficult to identify. The clearest exception is the microburst observed at 00:40:30 UT shown in Supplementary Figure S2. The three SAMPEX instruments' integral response make it difficult to infer the energy of the precipitating electrons—we can only claim that some of the electrons had a >1 MeV energy. Furthermore, the SAMPEX instruments show signs of time-energy dispersion. However, we are unable to reliably verify dispersion because the time synchronization between instruments was of order 1 second—longer than the theoretical sub-second energy dispersion.

4 Discussion

This event shows strong evidence of EMIC-driven IPA concurrent with >1 MeV electron microbursts. The EMIC wave was observed throughout central Canada for almost 2 hours. The wave precipitated 10 s keV protons in a localized patch which then generated the IPA light—confirmed by the white-light observed by THEMIS-TPAS and the H_β light observed by MSP-GILL. The wave also precipitated intense and rapid >1 MeV electron microbursts that SAMPEX observed directly above the IPA.

While Miyoshi et al. (2008) and Jordanova et al. (2008), and others show that quasilinear diffusion can model the gradual EMIC-driven relativistic electron precipitation, it is unable to model the intense sub-second relativistic microbursts studied here. Nonlinear EMIC-electron scattering models are probably needed. Albert and Bortnik (2009) show that nonlinear interactions between electrons and monochromatic EMIC waves lead to rapid electron transport in pitch angle (and negligible transport in energy). The scattering efficiency of relativistic electrons is strongly dependent on the gyrophase difference between the wave and particle and on the inhomogeneity parameter. Albert and Bortnik (2009) describe the inhomogeneity parameter as quantifying the strength of the EMIC wave relative to the inhomogeneity of the magnetospheric plasma and magnetic field.

Omura and Zhao (2012) extended this work from a monochromatic wave to rising tones, generated by the EMIC triggered emission mechanism (e.g., Grison et al., 2013; Sakaguchi et al., 2013). The authors found that the most effective EMIC-MeV electron scattering occurs with EMIC rising tones and repeated encounters with the wave as the electrons bounce: the EMIC wave is relatively stationary compared to a bouncing MeV electron. Omura and Zhao (2013) applied this theory to model EMIC-driven MeV microbursts. Here, the authors found that EMIC rising tones are very efficient at trapping relativistic electrons and

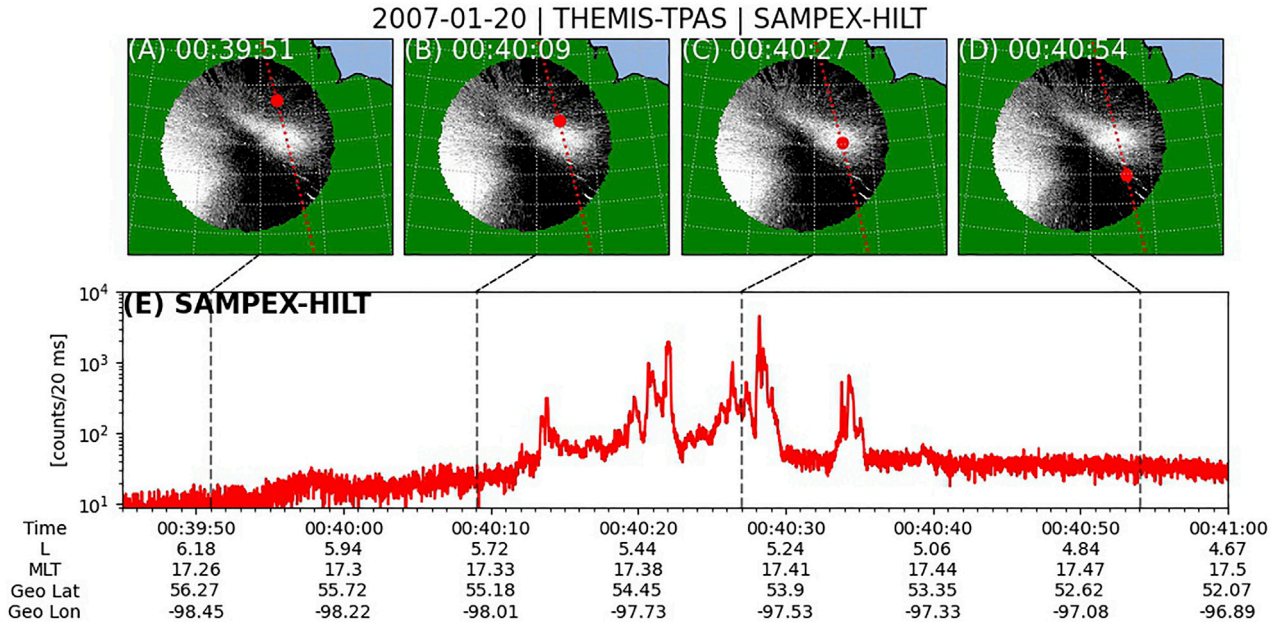

FIGURE 3
Select ASI images, and relativistic electron microbursts observed during the conjunction. **(A–D)** show select THEMIS ASI images from The Pas mapped to 110 km altitude. The SAMPEX footprint and its instantaneous position are shown by the dotted red line and the large red circle. The intensity bounds are identical between the images. **(E)** shows the SAMPEX-HILT time series with vertical guides at times that correspond to the ASI images in **(A–D)**. The minor ticks are at every second. The HILT instrument observed microbursts only when it passed above the proton aurora.

transporting them into the loss cone when the inhomogeneity parameter is less than one. The authors simulated an EMIC wave that propagated away from the magnetic equator to higher magnetic latitudes for 37 s. As the electrons bounced (with a sub-second bounce period), they repeatedly passed through and resonated with the wave for ≈ 20 ms. This led to efficient pitch angle transport of the resonant electrons into the loss cone. Figure 8b in Omura and Zhao (2013) shows an envelope of precipitating electrons with intense subsecond electron enhancements superposed; thus, the authors classified them as microbursts.

Thus, our observations are theoretically supported by Omura and Zhao (2013)'s results. Nonlinear wave-particle interactions between EMIC rising tones and electrons are necessary to generate these microbursts. Other studies including Nakamura et al. (2019), and Zhu et al. (2020) also presented evidence of nonlinear scattering of electron by EMIC rising tones that resulted in sub-minute flux variations observed by the Van Allen Probes (Mauk et al., 2012). That said, given that EMIC rising tones are necessary for nonlinear microburst scattering, our observations do not show clear EMIC rising tones. This is unsurprising, because ground-based observations of EMIC rising tones are rare—likely explained by the smoothing of the frequency dispersion during the propagation to the ground. In fact, Nomura et al. (2016) claims to be the first to have find EMIC rising tones on the ground.

We consider one final scenario: collocated EMIC and chorus waves. In this case, the EMIC waves were responsible for the IPA while the chorus waves were responsible for microbursts. While there were no direct equatorial wave measurements in this L-MLT region at this time, the MSP-GILL can infer the presence of 10 s keV electrons that are associated with lower-band chorus (Thorne et al., 2010). The green-to-blue MSP ratio is a good proxy for the precipitating electron energy spectrum: higher green-to-blue ratios correspond to lower energy electron precipitation (Rees and Luckey, 1974; Shepherd et al., 1996). The keograms in Figure 2 show an emission in the green but not the blue line. The large green-to-blue ratio indicates an absence of 10 s keV electron precipitation and thus suggest an absence of lower-band chorus waves that are capable of scattering MeV electrons.

The chorus-microburst model is admittedly very simple and widely accepted. But, our results suggest that there are multiple ways to scatter microbursts. Perhaps this is unsurprising, given that microbursts are broadly defined by their intensity and sub-second duration—so we would classify any wave-particle interaction capable of producing rapid precipitation as microbursts.

In conclusion, our observations show EMIC-driven precipitation of both 10 s keV protons that resulted in IPA light, and >1 MeV electron microbursts. Since relativistic electrons were not observed above the full extent of the

proton aurora, this means that the relativistic microburst electrons are episodic: a very specific triggering condition must have been met. Douma et al. (2018) showed an example of EMIC-driven microbursts, but the waves and MeV electrons were observed in opposite hemispheres, and no proton aurora was observed to localize the EMIC wave. Thus, our event is arguably the strongest evidence yet of nonlinear interactions between EMIC waves and electrons, leading to microburst precipitation. Our results are theoretically supported, despite the scant observational evidence in the published literature. Further, this study shows the indispensable utility of ground-based observations to gain a more comprehensive understanding of wave-particle interactions.

Data availability statement

Publicly available datasets were analyzed in this study. This data can be found here: CARISMA: https://www.carisma.ca/carisma-data-repository, THEMIS: https://data.phys.ucalgary.ca/sort_by_project/THEMIS/asi/MSP: https://data.phys.ucalgary.ca/sort_by_project/GO-Canada/GO-Storm/msp/IDLsav/SAMPEX: https://izw1.caltech.edu/sampex/DataCenter/.

Author contributions

MS, BG-L, KM, and AH first conceived the idea to look for SAMPEX-THEMIS ASI conjunctions. Both KH and YM first highlighted the uniqueness of this conjunction. AH wrote the draft introduction and MS wrote the rest of the manuscript. BG-L made Figure 2 and MS made the other plots. JL, ED, ES, and DG provided the THEMIS ASI and MSP data and expertise. JB and ML provided the SAMPEX data and analysis support. LB helped analyze the SAMPEX microburst observations. IM provided the CARISMA data. All authors contributed to manuscript revision, read, and approved the submitted version.

Funding

MS and BG-L acknowledge the support provided by the NASA Postdoctoral Program at the NASA's Goddard Space Flight Center, administered by Oak Ridge Associated Universities under contract with NASA. AH was supported in part by the Goddard Internal Funding Model which funds the Space Precipitation Impacts team with grant HISFM21. LB was supported by NASA H-SR award #80NSSC21K1682. YM was supported by JSPS 16H06286, 20H01959, and 21H04526.

Acknowledgments

This work was also in part inspired by preparation work for the LAMP rocket mission (NNH17ZDA001N-HTIDeS), and the ISSI Team "Dynamics of Electromagnetic Ion Cyclotron Wave Activity in the Earth's Magnetosphere". CARISMA is operated by the University of Alberta, funded by the Canadian Space Agency. The auroral data was in part analyzed using the aurora-asi-lib library which can be found at https://aurora-asi-lib.readthedocs.io/ and is archived at https://doi.org/10.5281/zenodo.4746446.

Conflict of interest

The authors declare that the research was conducted in the absence of any commercial or financial relationships that could be construed as a potential conflict of interest.

Publisher's note

Supplementary material

The Supplementary Material for this article can be found online at: https://www.frontiersin.org/articles/10.3389/fspas.2022.975123/full#supplementary-material

References

Albert, J., and Bortnik, J. (2009). Nonlinear interaction of radiation belt electrons with electromagnetic ion cyclotron waves. *Geophys. Res. Lett.* 36, L12110. doi:10.1029/2009gl038904

Anderson, K. A., and Milton, D. W. (1964). Balloon observations of x rays in the auroral zone: 3. High time resolution studies. *J. Geophys. Res. (1896-1977)* 69, 4457–4479. doi:10.1029/JZ069i021p04457

Baker, D., Mazur, J., and Mason, G. (2012). SAMPEX to reenter atmosphere: Twenty-year mission will end. *Space weather.* 10. doi:10.1029/2012sw000804

Baker, D. N., Mason, G. M., Figueroa, O., Colon, G., Watzin, J. G., and Aleman, R. M. (1993). An overview of the solar anomalous, and magnetospheric particle explorer (SAMPEX) mission. *IEEE Trans. Geosci. Remote Sens.* 31, 531–541. doi:10.1109/36.225519

Blum, L., Bonnell, J., Agapitov, O., Paulson, K., and Kletzing, C. (2017). Emic wave scale size in the inner magnetosphere: Observations from the dual van allen probes. *Geophys. Res. Lett.* 44, 1227–1233. doi:10.1002/2016gl072316

Blum, L., Li, X., and Denton, M. (2015). Rapid MeV electron precipitation as observed by SAMPEX/HILT during high-speed stream-driven storms. *J. Geophys. Res. Space Phys.* 120, 3783–3794. doi:10.1002/2014ja020633

Blum, L. W., MacDonald, E. A., Clausen, L. B. N., and Li, X. (2012). A comparison of magnetic field measurements and a plasma-based proxy to infer emic wave distributions at geosynchronous orbit. *J. Geophys. Res.* 117. doi:10.1029/2011JA017474

Bortnik, J., Albert, J. M., Artemyev, A., Li, W., Jun, C.-W., Grach, V. S., et al. (2022). Amplitude dependence of nonlinear precipitation blocking of relativistic electrons by large amplitude emic waves. *Geophys. Res. Lett.* 49, e2022GL098365. doi:10.1029/2022gl098365

Bortnik, J., Thorne, R., and Inan, U. S. (2008). Nonlinear interaction of energetic electrons with large amplitude chorus. *Geophys. Res. Lett.* 35, L21102. doi:10.1029/2008gl035500

[Dataset] Boscher, D., Bourdarie, S., O'Brien, P., Guild, T., and Shumko, M. (2012). *Irbem-lib library*.

Capannolo, L., Li, W., Spence, H., Johnson, A. T., Shumko, M., Sample, J., et al. (2021). Energetic electron precipitation observed by firebird-ii potentially driven by emic waves: Location, extent, and energy range from a multievent analysis. *Geophys. Res. Lett.* 48, e2020GL091564. doi:10.1029/2020GL091564

Chen, L., Breneman, A. W., Xia, Z., and Zhang, X.-j. (2020). Modeling of bouncing electron microbursts induced by ducted chorus waves. *Geophys. Res. Lett.* 47, e2020GL089400. doi:10.1029/2020gl089400

Claudepierre, S. G., Ma, Q., Bortnik, J., O'Brien, T. P., Fennell, J. F., and Blake, J. B. (2020). Empirically estimated electron lifetimes in the earth's radiation belts: Comparison with theory. *Geophys. Res. Lett.* 47, e2019GL086056. doi:10.1029/2019gl086056

Cook, W. R., Cummings, A. C., Cummings, J. R., Garrard, T. L., Kecman, B., Mewaldt, R. A., et al. (1993). Pet: A proton/electron telescope for studies of magnetospheric, solar, and galactic particles. *IEEE Trans. Geosci. Remote Sens.* 31, 565–571. doi:10.1109/36.225523

Cornwall, J. M. (1965). Cyclotron instabilities and electromagnetic emission in the ultra low frequency and very low frequency ranges. *J. Geophys. Res. (1896-1977)* 70, 61–69. doi:10.1029/JZ070i001p00061

Davidson, G. T. (1965). Expected spatial distribution of low-energy protons precipitated in the auroral zones. *J. Geophys. Res.* 70, 1061–1068. doi:10.1029/jz070i005p01061

Donovan, E., Mende, S., Jackel, B., Frey, H., Syrjäsuo, M., Voronkov, I., et al. (2006). The themis all-sky imaging array—System design and initial results from the prototype imager. *J. Atmos. Solar-Terrestrial Phys.* 68, 1472–1487. doi:10.1016/j.jastp.2005.03.027

Douma, E., Rodger, C. J., Blum, L. W., and Clilverd, M. A. (2017). Occurrence characteristics of relativistic electron microbursts from SAMPEX observations. *J. Geophys. Res. Space Phys.* 122, 8096–8107. doi:10.1002/2017JA024067

Douma, E., Rodger, C. J., Clilverd, M. A., Hendry, A. T., Engebretson, M. J., and Lessard, M. R. (2018). Comparison of relativistic microburst activity seen by SAMPEX with ground-based wave measurements at Halley, Antarctica. *J. Geophys. Res. Space Phys.* 123, 1279–1294. doi:10.1002/2017JA024754

Fang, X., Liemohn, M. W., Kozyra, J. U., and Solomon, S. C. (2004). Quantification of the spreading effect of auroral proton precipitation. *J. Geophys. Res.* 109, A04309. doi:10.1029/2003ja010119

Gallardo-Lacourt, B., Frey, H., and Martinis, C. (2021). Proton aurora and optical emissions in the subauroral region. *Space Sci. Rev.* 217, 10–36. doi:10.1007/s11214-020-00776-6

Gary, S. P., Thomsen, M. F., Yin, L., and Winske, D. (1995). Electromagnetic proton cyclotron instability: Interactions with magnetospheric protons. *J. Geophys. Res.* 100, 21961–21972. doi:10.1029/95JA01403

Grach, S., VeronikaDemekhov, G., and Andrei (2020). Precipitation of relativistic electrons under resonant interaction with electromagnetic ion cyclotron wave packets. *J. Geophys. Res. Space Phys.* 125, e2019JA027358. doi:10.1029/2019ja027358

Grach, V. S., Demekhov, A. G., and Larchenko, A. V. (2021). Resonant interaction of relativistic electrons with realistic electromagnetic ion–cyclotron wave packets. *Earth Planets Space* 73, 129–217. doi:10.1186/s40623-021-01453-w

Grison, B., Santolik, O., Cornilleau-Wehrlin, N., Masson, A., Engebretson, M., Pickett, J., et al. (2013). Emic triggered chorus emissions in cluster data. *J. Geophys. Res. Space Phys.* 118, 1159–1169. doi:10.1002/jgra.50178

Halford, A. J., Fraser, B. J., Morley, S. K., Elkington, S. R., and Chan, A. A. (2016). Dependence of emic wave parameters during quiet, geomagnetic storm, and geomagnetic storm phase times. *J. Geophys. Res. Space Phys.* 121, 6277–6291. doi:10.1002/2016JA022694

Harris, S., Mende, S., Angelopoulos, V., Rachelson, W., Donovan, E., Jackel, B., et al. (2009). Themis ground based observatory system design. *THEMIS Mission* 2009, 213–233. doi:10.1007/978-0-387-89820-9_10

Hirsch, M. (2016). pymap3d: Python 3d coordinate conversions for geospace. doi:10.5281/zenodo.213676

[Dataset] Jackel, B. (2005). Mpa: Meridian photometer array. Avalilable at: https://aurora.phys.ucalgary.ca/norstar/msp/inst.html (Accessed 06 15.2022).

Jacobs, J., Kato, Y., Matsushita, S., and Troitskaya, V. (1964). Classification of geomagnetic micropulsations. *J. Geophys. Res.* 69, 180–181. doi:10.1029/jz069i001p00180

Jordanova, V. K., Albert, J., and Miyoshi, Y. (2008). Relativistic electron precipitation by emic waves from self – consistent global simulations. *J. Geophys. Res.* 113. doi:10.1029/2008JA013239

Jordanova, V. K. (2007). Modeling geomagnetic storm dynamics: New results and challenges. *J. Atmos. Sol. – Terr. Phys.* 69, 56–66. doi:10.1016/j.jastp.2006.06.016

Kawamura, M., Sakanoi, T., Fukizawa, M., Miyoshi, Y., Hosokawa, K., Tsuchiya, F., et al. (2021). Simultaneous pulsating aurora and microburst observations with ground-based fast auroral imagers and cubesat firebird-ii. *Geophys. Res. Lett.* 48, e2021GL094494. doi:10.1029/2021gl094494

Kennel, C. F., and Petschek, H. (1966). Limit on stably trapped particle fluxes. *J. Geophys. Res.* 71, 1–28. doi:10.1029/jz071i001p00001

Khazanov, G., Sibeck, D., Tel'Nikhin, A., and Kronberg, T. (2014). Relativistic electron precipitation events driven by electromagnetic ion-cyclotron waves. *Phys. Plasmas* 21, 082901. doi:10.1063/1.4892185

Kim, H., Hwang, J., Park, J., Miyashita, Y., Shiokawa, K., Mann, I. R., et al. (2018). Large-scale ducting of pc1 pulsations observed by swarm satellites and multiple ground networks. *Geophys. Res. Lett.* 45 (12), 703712–12. doi:10.1029/2018GL080693

Kivelson, M. G., Kivelson, M. G., and Russell, C. T. (1995). *Introduction to space physics*. Cambridge: Cambridge University Press.

Klecker, B., Hovestadt, D., Scholer, M., Arbinger, H., Ertl, M., Kastele, H., et al. (1993). Hilt: A heavy ion large area proportional counter telescope for solar and anomalous cosmic rays. *IEEE Trans. Geosci. Remote Sens.* 31, 542–548. doi:10.1109/36.225520

Kubota, Y., and Omura, Y. (2017). Rapid precipitation of radiation belt electrons induced by emic rising tone emissions localized in longitude inside and outside the plasmapause. *J. Geophys. Res. Space Phys.* 122, 293–309. doi:10.1002/2016ja023267

Kubota, Y., Omura, Y., and Summers, D. (2015). Relativistic electron precipitation induced by emic-triggered emissions in a dipole magnetosphere. *J. Geophys. Res. Space Phys.* 120, 4384–4399. doi:10.1002/2015ja021017

Lorentzen, K., Blake, J., Inan, U., and Bortnik, J. (2001). Observations of relativistic electron microbursts in association with vlf chorus. *J. Geophys. Res.* 106, 6017–6027. doi:10.1029/2000ja003018

Lyons, L. R., and Thorne, R. M. (1973). Equilibrium structure of radiation belt electrons. *J. Geophys. Res.* 78, 2142–2149. doi:10.1029/ja078i013p02142

Mann, I., Milling, D., Rae, I., Ozeke, L., Kale, A., Kale, Z., et al. (2008). The upgraded carisma magnetometer array in the themis era. *Space Sci. Rev.* 141, 413–451. doi:10.1007/s11214-008-9457-6

Mann, I. R., Usanova, M. E., Murphy, K., Robertson, M. T., Milling, D. K., Kale, A., et al. (2014). Spatial localization and ducting of emic waves: Van allen probes and ground-based observations. *Geophys. Res. Lett.* 41, 785–792. doi:10.1002/2013GL058581

Mason, G. M., Hamilton, D. C., Walpole, P. H., Heuerman, K. F., James, T. L., Lennard, M. H., et al. (1993). Leica: A low energy ion composition analyzer for the study of solar and magnetospheric heavy ions. *IEEE Trans. Geosci. Remote Sens.* 31, 549–556. doi:10.1109/36.225521

Mauk, B., Fox, N. J., Kanekal, S., Kessel, R., Sibeck, D., and Ukhorskiy, a. A. (2012). "Science objectives and rationale for the radiation belt storm probes mission," in *The van allen Probes mission* (Berlin, Germany: Springer), 3–27.

Mende, S., Harris, S., Frey, H., Angelopoulos, V., Russell, C., Donovan, E., et al. (2009). The themis array of ground-based observatories for the study of auroral substorms. *THEMIS Mission* 2009, 357–387. doi:10.1007/978-0-387-89820-9_16

Meredith, N. P., Horne, R. B., Shen, X.-C., Li, W., and Bortnik, J. (2020). Global model of whistler mode chorus in the near-equatorial region (– λ m– ¡ 18). *Geophys. Res. Lett.* 47, e2020GL087311. doi:10.1029/2020gl087311

Miyoshi, Y., Saito, S., Kurita, S., Asamura, K., Hosokawa, K., Sakanoi, T., et al. (2020). Relativistic electron microbursts as high-energy tail of pulsating aurora electrons. *Geophys. Res. Lett.* 47, e2020GL090360. doi:10.1029/2020GL090360

Miyoshi, Y., Saito, S., Seki, K., Nishiyama, T., Kataoka, R., Asamura, K., et al. (2015). Relation between fine structure of energy spectra for pulsating aurora

electrons and frequency spectra of whistler mode chorus waves. *J. Geophys. Res. Space Phys.* 120, 7728–7736. doi:10.1002/2015ja021562

Miyoshi, Y., Sakaguchi, K., Shiokawa, K., Evans, D., Albert, J., Connors, M., et al. (2008). Precipitation of radiation belt electrons by emic waves, observed from ground and space. *Geophys. Res. Lett.* 35, L23101. doi:10.1029/2008gl035727

Mozer, F., Agapitov, O., Blake, J., and Vasko, I. (2018). Simultaneous observations of lower band chorus emissions at the equator and microburst precipitating electrons in the ionosphere. *Geophys. Res. Lett.* 45, 511–516. doi:10.1002/2017gl076120

Nakamura, S., Omura, Y., Kletzing, C., and Baker, D. N. (2019). Rapid precipitation of relativistic electron by EMIC rising-tone emissions observed by the Van Allen Probes. *J. Geophys. Res. Space Phys.* 124, 6701–6714. doi:10.1029/2019JA026772

Nishimura, Y., Bortnik, J., Li, W., Lyons, L., Donovan, E., Angelopoulos, V., et al. (2014). Evolution of nightside subauroral proton aurora caused by transient plasma sheet flows. *J. Geophys. Res. Space Phys.* 119, 5295–5304. doi:10.1002/2014ja020029

Nomura, R., Shiokawa, K., Omura, Y., Ebihara, Y., Miyoshi, Y., Sakaguchi, K., et al. (2016). Pulsating proton aurora caused by rising tone pc1 waves. *J. Geophys. Res. Space Phys.* 121, 1608–1618. doi:10.1002/2015JA021681

O'Brien, T., Lorentzen, K., Mann, I., Meredith, N., Blake, J., Fennell, J., et al. (2003). Energization of relativistic electrons in the presence of ulf power and mev microbursts: Evidence for dual ulf and vlf acceleration. *J. Geophys. Res.* 108, 1329. doi:10.1029/2002ja009784

Omura, Y., and Zhao, Q. (2012). Nonlinear pitch angle scattering of relativistic electrons by emic waves in the inner magnetosphere. *J. Geophys. Res.* 117. doi:10.1029/2012ja017943

Omura, Y., and Zhao, Q. (2013). Relativistic electron microbursts due to nonlinear pitch angle scattering by emic triggered emissions. *J. Geophys. Res. Space Phys.* 118, 5008–5020. doi:10.1002/jgra.50477

Parks, G. K. (1967). Spatial characteristics of auroral-zone x-ray microbursts. *J. Geophys. Res. (19641896-1977)* 72, 215–226. doi:10.1029/JZ072i001p00215

Qin, M., Hudson, M., Millan, R., Woodger, L., and Shekhar, S. (2018). Statistical investigation of the efficiency of emic waves in precipitating relativistic electrons. *J. Geophys. Res. Space Phys.* 123, 6223–6230. doi:10.1029/2018ja025419

Rees, M., and Luckey, D. (1974). Auroral electron energy derived from ratio of spectroscopic emissions 1. model computations. *J. Geophys. Res.* 79, 5181–5186. doi:10.1029/ja079i034p05181

Remya, B., Tsurutani, B., Reddy, R., Lakhina, G., and Hajra, R. (2015). Electromagnetic cyclotron waves in the dayside subsolar outer magnetosphere generated by enhanced solar wind pressure: Emic wave coherency. *J. Geophys. Res. Space Phys.* 120, 7536–7551. doi:10.1002/2015ja021327

Saikin, A., Zhang, J.-C., Allen, R., Smith, C., Kistler, L., Spence, H., et al. (2015). The occurrence and wave properties of h+-he+-and o+-band emic waves observed by the van allen probes. *J. Geophys. Res. Space Phys.* 120, 7477–7492. doi:10.1002/2015ja021358

Saito, S., Miyoshi, Y., and Seki, K. (2012). Relativistic electron microbursts associated with whistler chorus rising tone elements: Gemsis-rbw simulations. *J. Geophys. Res.* 117. doi:10.1029/2012ja018020

Sakaguchi, K., Kasahara, Y., Shoji, M., Omura, Y., Miyoshi, Y., Nagatsuma, T., et al. (2013). Akebono observations of emic waves in the slot region of the radiation belts. *Geophys. Res. Lett.* 40, 5587–5591. doi:10.1002/2013gl058258

Sakaguchi, K., Shiokawa, K., Miyoshi, Y., Otsuka, Y., Ogawa, T., Asamura, K., et al. (2008). Simultaneous appearance of isolated auroral arcs and pc 1 geomagnetic pulsations at subauroral latitudes. *J. Geophys. Res.* 113. doi:10.1029/2007ja012888

Shepherd, M. G., Gattinger, R. L., and Jones, A. V. (1996). Observation and analysis of ni 520.0 nm auroral emissions. *J. Atmos. Terr. Phys.* 58, 579–599. doi:10.1016/0021-9169(95)00059-3

Shoji, M., and Omura, Y. (2011). Simulation of electromagnetic ion cyclotron triggered emissions in the earth's inner magnetosphere. *J. Geophys. Res.* 116. doi:10.1029/2010ja016351

Shumko, M. (2022). aurora-asi-lib: easily download, plot, animate, and analyze aurora all sky imager (ASI) data. doi:10.5281/zenodo.4746446

Shumko, M., Blum, L. W., and Crew, A. B. (2021). Duration of individual relativistic electron microbursts: A probe into their scattering mechanism. *Geophys. Res. Lett.* 48, e2021GL093879. doi:10.1029/2021gl093879

Shumko, M., Johnson, A., O'Brien, T. P., Turner, D. L., Greeley, A. D., Sample, J. G., et al. (2020a). Electron microburst size distribution derived with AeroCube-6. *J. Geophys. Res. Space Phys.* 125, e2019JA027651. doi:10.1029/2019JA027651

Shumko, M., Johnson, A. T., Sample, J. G., Griffith, B. A., Turner, D. L., O'Brien, T. P., et al. (2020b). Electron microburst size distribution derived with AeroCube-6. *J. Geophys. Res. Space Phys.* 125, e2019JA027651. doi:10.1029/2019ja027651

Shumko, M., Turner, D. L., O'Brien, T. P., Claudepierre, S. G., Sample, J., Hartley, D. P., et al. (2018). Evidence of microbursts observed near the equatorial plane in the outer van allen radiation belt. *Geophys. Res. Lett.* 45, 8044–8053. doi:10.1029/2018GL078451

Spasojević, M., Frey, H. U., Thomsen, M. F., Fuselier, S. A., Gary, S. P., Sandel, B. R., et al. (2004). The link between a detached subauroral proton arc and a plasmaspheric plume. *Geophys. Res. Lett.* 31, L04803. doi:10.1029/2003GL018389

Summers, D. (2005). Quasi-linear diffusion coefficients for field-aligned electromagnetic waves with applications to the magnetosphere. *J. Geophys. Res.* 110. doi:10.1029/2005ja011159

Summers, D., Thorne, R. M., and Xiao, F. (1998). Relativistic theory of wave-particle resonant diffusion with application to electron acceleration in the magnetosphere. *J. Geophys. Res.* 103, 20487–20500. doi:10.1029/98ja01740

Teng, S., Tao, X., Xie, Y., Zonca, F., Chen, L., Fang, W., et al. (2017). Analysis of the duration of rising tone chorus elements. *Geophys. Res. Lett.* 44, 12–074. doi:10.1002/2017gl075824

Thébault, E., Finlay, C. C., Beggan, C. D., Alken, P., Aubert, J., Barrois, O., et al. (2015). International geomagnetic reference field: The 12th generation. *Earth Planets Space* 67, 158. doi:10.1186/s40623-015-0313-0

Thorne, R. M., Ni, B., Tao, X., Horne, R. B., and Meredith, N. P. (2010). Scattering by chorus waves as the dominant cause of diffuse auroral precipitation. *Nature* 467, 943–946. doi:10.1038/nature09467

Thorne, R. M., O'Brien, T., Shprits, Y., Summers, D., and Horne, R. B. (2005). Timescale for mev electron microburst loss during geomagnetic storms. *J. Geophys. Res.* 110. doi:10.1029/2004ja010882

Unick, C. W., Donovan, E., Connors, M., and Jackel, B. (2017). A dedicated H-beta meridian scanning photometer for proton aurora measurement. *J. Geophys. Res. Space Phys.* 122, 753–764. doi:10.1002/2016ja022630

Van Allen, J. A. (1959). The geomagnetically trapped corpuscular radiation. *J. Geophys. Res. (1896-1977)* 64, 1683–1689. doi:10.1029/JZ064i011p01683

Vernov, S., and Chudakov, A. (1960). Investigation of radiation in outer space. *Sov. Phys. Usp.* 3, 230–250. doi:10.1070/pu1960v003n02abeh003269

Virtanen, P., Gommers, R., Oliphant, T. E., Haberland, M., Reddy, T., Cournapeau, D., et al. (2020). SciPy 1.0: Fundamental algorithms for scientific computing in Python. *Nat. Methods* 17, 261–272. doi:10.1038/s41592-019-0686-2

Winckler, J. R., Peterson, L., Arnoldy, R., and Hoffman, R. (1958). X-rays from visible aurorae at minneapolis. *Phys. Rev.* 110, 1221–1231. doi:10.1103/PhysRev.110.1221

Woodger, L., Halford, A., Millan, R., McCarthy, M., Smith, D., Bowers, G., et al. (2015). A summary of the barrel campaigns: Technique for studying electron precipitation. *J. Geophys. Res. Space Phys.* 120, 4922–4935. doi:10.1002/2014ja020874

Woodroffe, J. R., and Lysak, R. L. (2012). Ultra-low frequency wave coupling in the ionospheric alfvén resonator: Characteristics and implications for the interpretation of ground magnetic fields. *J. Geophys. Res.* 117. doi:10.1029/2011JA017057

Yahnin, A. G., Popova, T. A., Demekhov, A. G., Lubchich, A. A., Matsuoka, A., Asamura, K., et al. (2021). Evening side emic waves and related proton precipitation induced by a substorm. *J. Geophys. Res. Space Phys.* 126, e2020JA029091. doi:10.1029/2020JA029091

Zhang, J., Halford, A. J., Saikin, A. A., Huang, C.-L., Spence, H. E., Larsen, B. A., et al. (2016a). Emic waves and associated relativistic electron precipitation on 25–26 january 2013. *J. Geophys. Res. Space Phys.* 121, 11, 086086100. doi:10.1002/2016JA022918

Zhang, X.-J., Angelopoulos, V., Mourenas, D., Artemyev, A., Tsai, E., and Wilkins, C. (2022). Characteristics of electron microburst precipitation based on high-resolution elfin measurements. *JGR. Space Phys.* 127, e2022JA030509. doi:10.1029/2022ja030509

Zhang, X.-J., Li, W., Ma, Q., Thorne, R., Angelopoulos, V., Bortnik, J., et al. (2016b). Direct evidence for emic wave scattering of relativistic electrons in space. *J. Geophys. Res. Space Phys.* 121, 6620–6631. doi:10.1002/2016ja022521

Zhu, H., Chen, L., Claudepierre, S. G., and Zheng, L. (2020). Direct evidence of the pitch angle scattering of relativistic electrons induced by emic waves. *Geophys. Res. Lett.* 47, e2019GL085637. doi:10.1029/2019gl085637